Title:

Rotation-Invariant Ground-Motion as Directional Selection Operators: A Closed-Form Framework for RotD Response Spectra

Authors:

Rajesh Rupakhety[1]

Víctor M. Hernández-Aguirre[2]

[1] Earthquake Engineering Research Centre, Faculty of Civil and Environmental Engineering, University of Iceland, Austurvegur 2a, 800 Selfoss, Iceland

Email: rajesh@hi.is

[2] Earthquake Engineering Research Centre, Faculty of Civil and Environmental Engineering, University of Iceland, Austurvegur 2a, 800 Selfoss, Iceland

Email: victorh@hi.is

Preprint Statement

This manuscript is a preprint and has not undergone peer review.

The manuscript is currently under review in Earthquake Engineering and Structural Dynamics.

This version is posted on EarthArXiv to ensure transparency, accessibility, and timely dissemination of the research.

The final published version, if accepted, may differ from this preprint.

Date of Preprint Posting:
20 February 2026

Rotation-Invariant Ground-Motion as Directional Selection Operators: A Closed-Form Framework for RotD Response Spectra

Rajesh Rupakhety[1*], Victor Moises Hernández-Aguirre[1]

Abstract

Horizontal earthquake ground motion is inherently two-dimensional, yet most engineering applications rely on scalar intensity measures. Rotation-invariant response spectra such as RotD50, MaxRotD50, and RotD100 are widely used to remove dependence on sensor orientation. They are often treated as direction-free scalars, which they are not. In this study, directional pseudo-spectral acceleration is treated instead as a stochastic field on the circle. Rotation-invariant measures are interpreted as directional selection operators acting on that field. Building on empirical evidence that the squared directional response is strongly dominated by its first admissible angular harmonic, we derive closed-form approximations for RotD50, MaxRotD50, and RotD100. This removes the need for explicit directional sampling while making clear what directional information is retained by each operator. Validation against a large ground-motion dataset shows that the closed-form predictions are essentially unbiased across periods and preserve record-to-record variability. A key finding is that max-type rotation-invariant measures depend on an effective anisotropy that includes a stochastic contribution arising from directional peak variability, even when geometric anisotropy is weak. As a result, ratios such as RotD100/RotD50 can be elevated in motions that are nearly isotropic in the root mean square sense. The results identify anisotropy of pseudo-spectral acceleration (PSA), evaluated along the principal directions of root mean square response, as a latent directional state variable. It controls the behaviour of rotation-invariant measures and their ratios across records and periods. Rather than removing directionality, rotation-invariant operators transform it. Recognizing this distinction provides a more transparent and physically interpretable basis for the use of rotation-invariant intensity measures in ground-motion modelling and seismic design.

Keywords: rotation-invariant response spectra, peak factor, ground motion directionality

1. Introduction

In the horizontal plane, ground motion at a site is a two-component vector process whose intensity varies with the chosen orientation of the horizontal axes. This directional dependence reflects physical mechanisms such as rupture directivity, wave-propagation effects, and directional site response. Yet most engineering workflows, including ground-motion models (GMMs), probabilistic seismic hazard analysis (PSHA), record selection and scaling, and design-code procedures, rely on scalar intensity measures. Scalarization is practical: it simplifies conditioning in seismic hazard calculations, and aligns with long-standing earthquake-resistant design conventions that combine orthogonal structural demands using simple algebraic rules (e.g., ASCE/SEI 7-16, 2022; EC8 CEN, 2004).

Rotation-invariant response-spectrum measures, such as RotD50 and RotD100, are now widely used to support this scalarization. By aggregating directional response over all azimuths, they remove the arbitrary dependence of scalar measures on sensor orientation. In common practice, rotation-invariant measures are computed by rotating the recorded horizontal pair through a dense angular grid, evaluating pseudo-spectral acceleration as a function of orientation, and applying an aggregation operator such as an angular median (RotD50) or an angular maximum (RotD100).

Rotation invariance, however, has often been implicitly conflated with direction-free representation. The numerical workflow, consisting of dense sampling in orientation followed by a statistic, encourages an implicit interpretation in which the directional response is treated as a collection of redundant samples and the rotation-invariant measure is viewed as a conventional statistic of those samples. This paper adopts a different interpretation. Directional pseudo-spectral acceleration is more naturally viewed as a structured stochastic field on the circle, and rotation-invariant measures are best understood as directional selection operators acting on that field.

[1] Earthquake Engineering Research Center, Faculty of Civil and Environmental Engineering, University of Iceland, Austurvegur 2a, 800 Selfoss, Iceland
* Corresponding author, rajesh@hi.is

Under this field-functional view, selection over direction is not equivalent to removing directional information. Max-type measures such as RotD100 are explicitly defined through directional selection and therefore cannot, in general, be assumed to behave as direction-free scalars, especially in workflows that later reintroduce directionality, for example through structural orientation or bidirectional demand combinations.

Building on the empirically verified low-dimensional angular structure of directional peak response established in Rupakhety and Hernádez-Aguirre (2026), this study addresses two questions. What directional information is fundamentally required to determine common rotation-invariant measures, and do different rotation-invariant operators preserve or suppress directional structure? To answer these questions, we derive closed-form approximations for RotD50, MaxRotD50, and RotD100 using a small set of quantities computed from the root mean squared (RMS) principal orthogonal pair of a record, together with an empirically grounded closure for unresolved stochastic anisotropy. The resulting framework eliminates the need for dense directional sampling rotation while making explicit the directional information preserved by each operator.

The paper proceeds from a review of existing component definitions to a field-functional formulation of rotation invariance, followed by closed-form derivation, its validation, and discussion of implications for engineering practice.

2 Background and prior work

Engineering applications have long relied on scalar horizontal intensity measures (IMs) to represent two-component excitation. Common choices include a single arbitrary component, the larger of the two recorded components, or the geometric mean of orthogonal components. While these definitions can yield similar median responses, they differ in dispersion. Beyer and Bommer (2006) systematically quantified relationships between medians and variabilities for a range of IMs, emphasizing the need for consistent component definitions.

A key motivation for rotation-invariant measures is not structural directionality per se, but the dependence of commonly used scalars, most notably the geometric mean of the two recorded horizontals, on the as-installed sensor azimuth. Boore et al. (2006) formalized orientation-independent measures by rotating the recorded horizontal pair through non-redundant angles and extracting percentiles, thereby defining scalars that are invariant to instrument orientation.

Boore (2010) introduced the RotDnn family of orientation-independent response spectra, which avoid geometric means and provide a logically ordered sequence from minimum to maximum across orientations at each period (e.g., RotD50 as the 50^{th} percentile or angular median; RotD100 as the 100^{th} percentile or angular maximum). Two properties emphasized in the RotDnn literature are central here. First, response spectra exhibit 180° periodicity with rotation angle. Second, the direction that maximizes response for RotD100 can vary rapidly with period, so the “maximum direction” is not a single physical direction shared across periods. These properties highlight that max-type rotation-invariant measures are constructed through directional selection at each period, rather than by averaging over orientations. Directional selection is intrinsic to these measures.

In parallel with the widespread use of median or average measures in ground-motion prediction, design provisions have increasingly emphasized maximum-direction spectral ordinates. Stewart et al. (2011) discuss representation of bidirectional ground motions in building codes and argue that RotD100-based provisions can be overly conservative for many structures. Poulos and Miranda(2022) similarly note that current U.S. design codes are based on RotD100 and argue that this choice can be conservative because it implicitly assumes alignment between the direction of maximum ground-motion intensity and the structure’s principal axes.

Within GMM development, the NGA-West1 generation (e.g., Chiou & Youngs, 2008) largely adopted an orientation-independent median measure based on rotated geometric means GMRotI50 (Boore et al., 2006).Following the NGA-West2 project, RotD50 became the predominant choice (e.g., Ancheta et al., 2014; Bozorgnia et al., 2014; Lanzano et al., 2019). However, earthquake resistant earthquake-resistant design in the United States generally prefers RotD100. To bridge this mismatch, empirical models for the ratio SaRotD100/SaRotD50 have been proposed (Shahi & Baker, 2014). This ratio is theoretically bounded between 1 (unpolarized response) and $\sqrt{2}$ (completely polarized response). Because different stages of practice employ different IMs, a substantial literature has developed empirical conversion relationships between rotation-invariant measures Boore and Kishida (2017) updated relationships among common IMs using large datasets and showed that magnitude and distance dependence is generally modest compared to record-to-record variability.

Poulos and Miranda (2022) proposed MaxRotD50 to reflect the fact that many structures respond along two orthogonal principal axes. MaxRotD50 is defined as the median over orientations of the maximum of two

orthogonal spectral ordinates at each orientation. This construction is directly motivated by the probability of exceedance in at least one of two orthogonal directions.

The spread of PSA(θ) across orientations reflects physical mechanisms such as rupture directivity, radiation pattern, path effects, and directional site response. Well-documented examples include directional site resonances(Vidale et al., 1991), directional topographic site response (Spudich et al., 1996), and directivity-motivated modifications to attenuation relations (Somerville et al., 1997). These mechanisms motivate viewing PSA(θ) as a structured angular field rather than as a collection of redundant samples.

In practice RotD-type measures are almost exclusively implemented through dense rotation. Rupakhety and Sigbjörnsson (2013, 2014b, 2014a) present a different interpretation of rotation-invariant ground motions, especially RotD50 and strong-motion duration, relying on the invariant RMS response. Boore (2010) describes this rotation-based construction explicitly, including the 180° periodicity of response spectra; Poulos and Miranda (2022) similarly note that 1° increments are sufficient for stable MaxRotD-type computations. This numerical paradigm has shaped how rotation-invariant measures are commonly conceptualized as statistics of densely sampled orientations. A central motivation for the present study is to move beyond this numerical viewpoint by treating orientation-dependent response as a stochastic angular field and interpreting RotD-type quantities as selection functionals acting on that field. This interpretation becomes essential when moving from median-based measures to max-type or orthogonal selection operators.

3 Problem framing: rotation invariance as directional selection

At a fixed oscillator period, pseudo-spectral acceleration varies smoothly with orientation in the horizontal plane. Any rotation-invariant measure can therefore be interpreted as an operator acting on an underlying directional response field. From this perspective, rotation invariance does not imply loss of directional information. Instead, it specifies which directional features of the field are retained when a scalar measure is reported.

Within this framework, commonly used rotation-invariant measures differ in how they select from the directional field. RotD50 corresponds to a central tendency of directional response. MaxRotD50 corresponds to selection of favourable orthogonal orientations. RotD100 corresponds to selection of the extreme directional response. All three measures are invariant to the choice of coordinate system, but they preserve fundamentally different aspects of directional ground motion. This distinction has important implications. Measures based on central tendency suppress directional extremes and are relatively insensitive to weak anisotropy. In contrast, max-type measures emphasize directional modulation and respond strongly to both geometric and stochastic sources of anisotropy. As a result, max-type rotation-invariant measures do not behave as scalar equivalents of the full directional field.

Treating max-type invariants as drop-in scalar equivalents can therefore be conceptually inconsistent in workflows that later reintroduce directionality, for example by applying the same spectrum along two orthogonal structural axes and combining demands using simple algebraic rules or reduced orthogonal component rules. If a scalar measure already encodes directional selection, using it as if it was direction-free risks conflating baseline amplitude with directional variability.

4. Methodology: closed-form rotation-invariant measures

This section develops the conceptual framework introduced in Section 3 into a practical methodology for closed-form rotation-invariant intensity measures. The emphasis is on physical interpretation and on clarifying how rotation-invariant operators act on the directional pseudo-spectral acceleration field. The complete mathematical derivation is provided in Appendix A. All analyses are based on 2182 ground-motion records from the European Strong-Motion (ESM; Luzi et al., 2016) database. Details of record selection, preprocessing, and basic statistics are provided in Rupakhety and Hernández-Aguirre (2026) and are not repeated here.

4.1 Empirical structure of the directional field

Extensive diagnostics presented in Rupakhety and Hernández-Aguirre (2026) show that, at a fixed oscillator period, directional variations of PSA about its angular median exhibit low-dimensional structure. The angular dependence is strongly dominated by the first admissible harmonic imposed by π-periodicity, while higher-order angular content contributes a bounded remainder. This behaviour is observed consistently across records and periods. The essential directional information required to evaluate rotation-invariant measures is contained in a small number of parameters. As a result, rotation-invariant measures can be characterized without explicit sampling over orientation, provided that the dominant angular structure of the directional field is properly represented.

4.2 RMS geometry and directional selection

The dominant angular representation of PSA(θ) is governed by the RMS response geometry. The RMS response admits a pair of principal directions, separated by 90°, along which the RMS pseudo-acceleration attains its maximum and minimum values. Evaluating PSA along these directions defines an ordered orthogonal pair, $S_1 \geq S_2, \;\; S_i = PSA_i^2$.

From this pair, two invariants can be defined. The first invariant is a baseline level, $I = (S_1 + S_2)$. The second invariant, $\kappa = (S_1 - S_2)/(S_1 + S_2), \quad \kappa \in [0,1)$, termed as PSA anisotropy, quantifies the amplitude of directional modulation of the PSA field. Although it is derived from RMS principal directions, it should not be interpreted as geometric RMS anisotropy in the strict second-moment sense. It is defined in squared-PSA space and reflects directional modulation of PSA rather than second-moment geometry alone.

Figure 1 presents a visual summary of the modelling assumptions used to obtain closed-form rotation-invariant measures. The directional PSA field is decomposed into two contributing factors. The first is the RMS response geometry. It defines a preferred orthogonal basis and a geometric modulation level. The second is a direction-dependent peak-factor variability. It modulates the RMS field and can alter both the amplitude and the orientation of PSA relative to the RMS principal axes. This decomposition can be written in the form (see Paper 1) $PSA(\theta) = \sigma(\theta)\, p(\theta)$. where $\sigma(\theta)$ and $p(\theta)$ are respectively, the rms pseudo-acceleration and peak factor. The peak factor is represent as $\ln p(\theta) = \mu_p + \varepsilon(\theta)$, with μ_p and $\varepsilon(\theta)$ representing its median and fluctuation around the median, respectively.

In the top panels of Figure 1, the blue curve shows the computed directional PSA field, PSA(θ). The orange curve shows the PSA field that would result if the peak factor were direction independent, obtained by multiplying the RMS response as a function of orientation by a constant median peak factor μ_p. This construction isolates the contribution of RMS geometry from peak factor fluctuations. In the high-κ example, PSA extrema occur close to the RMS principal directions, and the constant-peak-factor field captures both the orientation and magnitude of directional amplification. When κ is small, this alignment breaks down. PSA extrema rotate away from the RMS principal directions, and the constant-peak-factor field substantially underestimates max-type response.

The bottom panels of Figure 1 show that, despite these differences in alignment and amplification, the directional PSA field remains well approximated by its first admissible harmonic in both regimes (dashed orange curves). This first-harmonic dominance holds even when RMS geometry alone does not control the direction or magnitude of PSA extremes. This structure forms the basis for the closed-form approximations developed in the following sections.

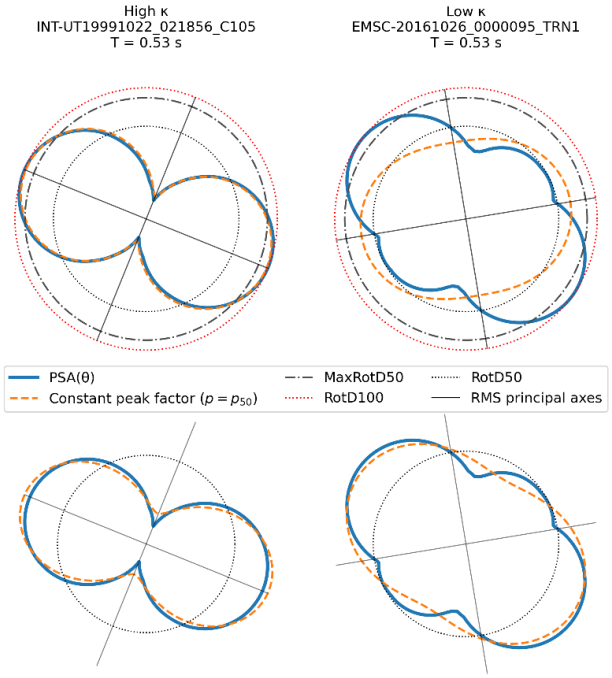

Figure 1 Directional PSA fields at T = 0.53 s for representative high- and low-anisotropy records. Top panels: computed PSA(θ) (blue) and the PSA field obtained from RMS response multiplied by a constant median peak factor (dashed orange). Bottom panels show computed PSA(θ) fields and first admissible harmonic approximations (dashed orange), demonstrating first-harmonic dominance in both anisotropy (κ) regimes.

4.3 Unresolved quadrature components of the directional PSA field

Figure 1 also highlights a fundamental limitation of representing PSA(θ) based solely on the principal orthogonal pair (I, κ). While the RMS principal directions determine the in-phase component of the dominant harmonic of PSA(θ), they do not uniquely determine the full harmonic state of the directional field. In particular, the orthogonal pair contains no information about the corresponding quadrature (out-of-phase) component of the first harmonic. Because max-type operators depend on the magnitude of directional modulation rather than on its alignment with the RMS principal directions, they are inherently sensitive to this unresolved quadrature component.

Figure 2 examines the statistical structure of the unresolved quadrature component and motivates the closure adopted in this study. Panel B represents the first-harmonic content of the directional peak-factor fluctuation field (ε)in coefficient space. The cloud of points is tightly clustered around the origin and approximately circular, indicating that peak-factor variability is weak on average and approximately isotropic The high-κ example lies primarily along the in-phase axis, reflecting dominance of RMS-aligned modulation. When κ is small, ε lies close to the quadrature axis. Directional modulation of PSA is then controlled primarily by the unresolved quadrature.

The distribution of the first-harmonic amplitude across records is shown in Panel C. The distribution is well described by a Rayleigh form with a stable median. When κ is large, representative records sample near this median amplitude. As κ decreases, effective sampling shifts toward the tail of the distribution. The consequence is systematic. Geometric predictors systematically under-estimate the magnitude of directional modulation relevant to max-type selection. Because MaxRotD50 and RotD100 select from different portions of this distribution, they amplify a typical amplitude of the peak factor fluctuation field differently.

4.4 Effective anisotropy closure and closed-form expressions

The observations summarized in Figures 1 and 2 motivate the introduction of an effective anisotropy that combines κ with a stochastic contribution. For max-type operators, effective anisotropy is defined as

$$\kappa_{eff,\,i} = \sqrt{\kappa^2 + \kappa_{\perp,\,i}^2}, \quad i \in \{50,100\} \tag{1}$$

Here $i \in \{50,100\}$ correspond MaxRotD50, and RotD50 operators, respectively. The stochastic term is given by $\kappa_{\perp,\,i} = c_i \rho_0$ where ρ_0 is the median of the Rayleigh distribution characterizing first-harmonic peak-factor variability (Figure 2C), and c_i are operator-specific inflation constants calibrated from data in the low κ regime. This construction ensures that effective anisotropy remains finite as $\kappa \to 0$, while reducing to the geometric contribution when κ is large. The rotation-invariant measures are then approximated by the following equations.

$$RotD50 \approx \sqrt{\frac{I}{2}} \tag{2}$$

$$MaxRotD50 \approx \sqrt{\frac{I}{2}}\sqrt{1 + \frac{\kappa_{eff,50}^2}{\sqrt{2}}} \tag{3}$$

$$RotD100 \approx \sqrt{\frac{I}{2}}\sqrt{1 + \frac{\kappa_{eff,100}^2}{\sqrt{2}}} \tag{4}$$

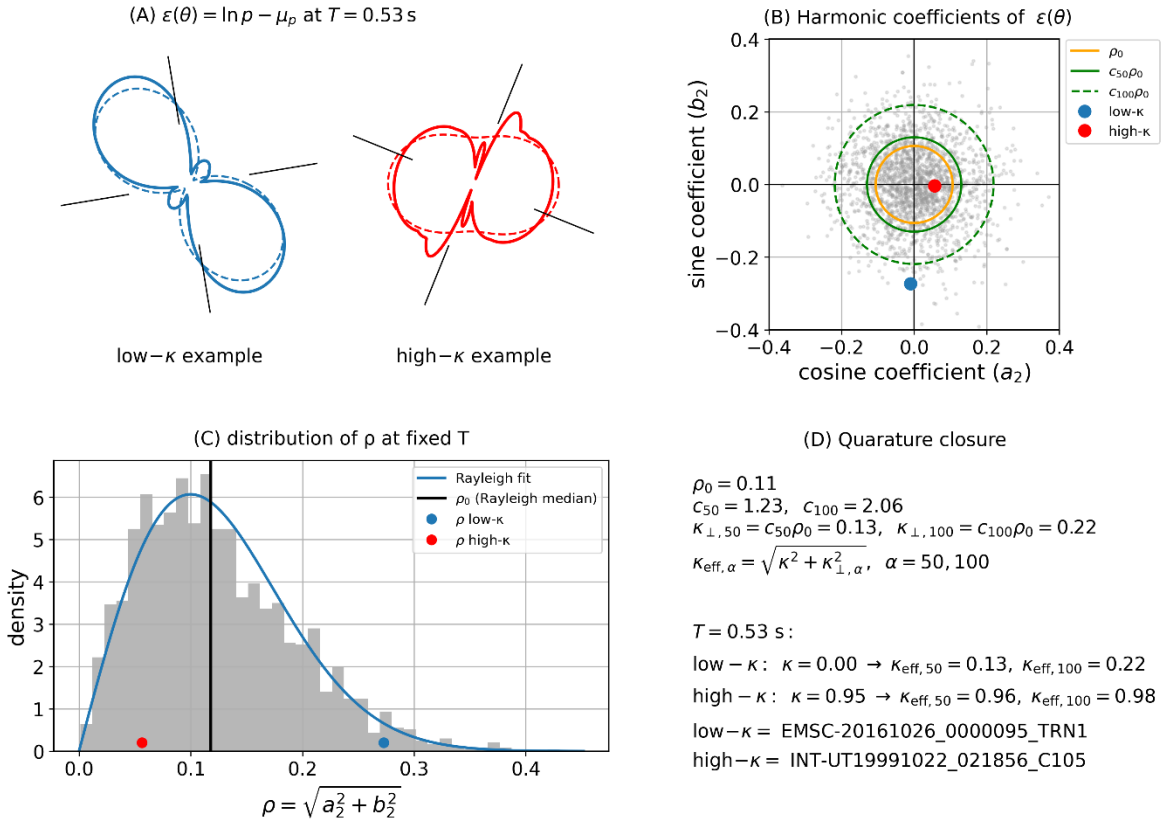

Figure 2. Illustration of the quadrature closure used to account for directional peak-factor variability at T = 0.53 s. ***(A)*** *Directional fluctuations of the logarithmic peak factor for representative low- and high-κ records.* ***(B)*** *Corresponding first-harmonic coefficients in phase space, highlighting the unobserved quadrature component relative to the RMS-aligned in-phase component.* ***(C)*** *Distribution of first-harmonic amplitudes across records at fixed period, well described by a Rayleigh model with a stable median.* ***(D)*** *Definition of operator-specific effective anisotropy, combining the PSA-based anisotropy parameter κ (defined in squared-PSA space) with a stochastic floor to account for unresolved quadrature variability in max-type rotation-invariant measures.*

5 Results

This section evaluates the accuracy and empirical robustness of the proposed closed-form formulation for rotation-invariant PSA. We focus on validating the empirical assumptions used in the framework and quantifying how the resulting approximations propagate into errors in rotation-invariant measures.

5.1 Validation of the first-harmonic approximation in squared PSA space

To assess the quality of first-harmonic approximation of PSA field, we quantify the magnitude of the neglected content using the sup-norm remainder in Equation (A12) in Appendix A. For comparison across records and periods, a normalized remainder is defined as

$$\tilde{\delta}_s = \frac{\delta_s}{a_0},$$

where a_0 is the overall level of the first-harmonic approximation. This normalized remainder provides a conservative, dimensionless measure of the truncation error induced by higher harmonics and nonlinear interactions. Figure 3 shows the distribution of $\tilde{\delta}_s$ across all records as a function of oscillator period. The median value remains modest over the full period range, with limited variability across records. The results show that even after the nonlinear transformation from directional peak factors to squared PSA, the angular structure of the response remains strongly dominated by the first harmonic, across records and periods.

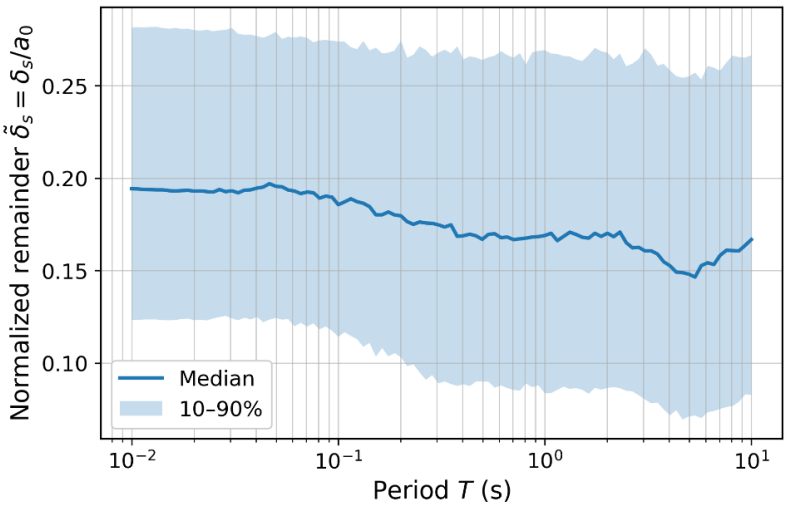

Figure 3. Distribution of normalized truncation error (higher-harmonic remainder) across all periods and records.

Figure 4 translates the truncation remainder in squared-PSA space into conservative bounds on PSA-level error for each rotation-invariant measure. For each record and period, the bounds shown correspond to the maximum relative error that could arise solely from replacing the full squared directional field by its first-harmonic projection. The bounds are modest, with median values on the order of 8 to 10% for RotD50, 6 to 8% for MaxRotD50, and 4 to 6% for RotD100.

The ordering of error bounds in the three rotation-invariant measures reflects intrinsic differences in operator sensitivity. Although RotD50 eliminates deterministic directional anisotropy at leading order, it is the most sensitive to residual higher-harmonic content in $S(\theta)$. Median-based operators are particularly exposed to such remainder structure because they depend on global rank ordering across directions. Small higher-harmonic perturbations can alter the angular ordering sufficiently to shift the median, producing a systematic truncation error. In contrast, max-type operators are dominated by the primary lobe of the directional response and are therefore less sensitive to distributed higher-mode content.

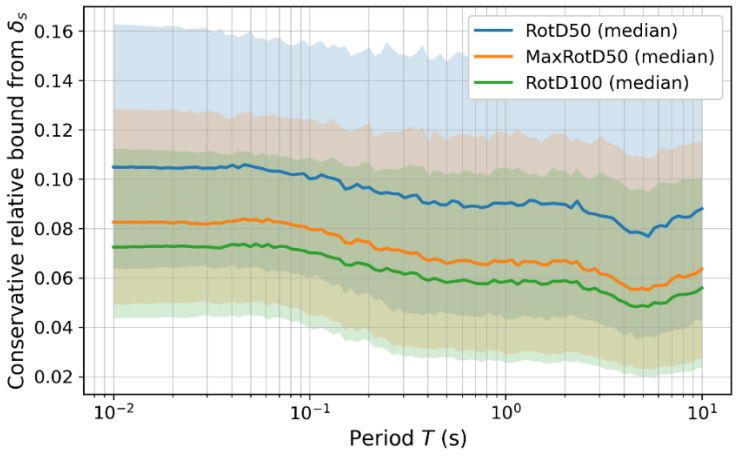

Figure 4. Median and 10th–90th percentile range of PSA-level error bounds for RotD50, MaxRotD50, and RotD100 as functions of period.

5.2 The effective anisotropy floor parameter

The stochastic portion of the effective anisotropy in Equation (1) is an inflation constant c, multiplied with a typical amplitude of peak-factor fluctuation amplitude (ρ_0) in its first harmonic projection. Rupakhety and Hernández-Aguirre (2026) shows that the Rayleigh scale parameter s of the $\varepsilon(\theta)$amplitude is only weakly dependent on oscillator period. We therefore estimate a typical amplitude of $\rho_0 = s\sqrt{2\ln 2}$. A period-independent value of $s = 0.09$ is adopted based on results in Rupakhety and Hernández-Aguirre (2026). The

inflation constant c_i is calibrated separately for MaxRotD50 and RotD100 using observations in the low-anisotropy regime. Calibration is performed by matching median empirical amplification to the corresponding closed-form prediction in this regime, ensuring unbiased behaviour $\kappa \to 0$. This constraint anchors the closure in observed low-anisotropy behaviour.

Figure 5 illustrates the calibration by comparing empirical amplification factors with closed-form predictions as functions of κ. For each operator, two reference models are shown in addition to the calibrated curve. The case $c_i = 0$ corresponds to constant peak factors. The case $c_i = 1$ represents unamplified peak-factor anisotropy entering directly into κ_{eff}. Both reference models underpredict observed amplification at low κ, indicating that nonlinear effects amplify the contribution of peak-factor variability beyond its nominal level. A geometric description alone is therefore insufficient in this regime. The calibrated models, obtained by matching median empirical amplification in the low-κ regime, closely match the observed median across the full anisotropy range. The resulting operator-specific constants are $c_{50} = 1.226$ and $c_{100} = 2.065$. A separate check confirmed that the calibrated constants do not introduce period-dependent bias. Median log-amplification residuals were found to lie within ±1% across the period range.

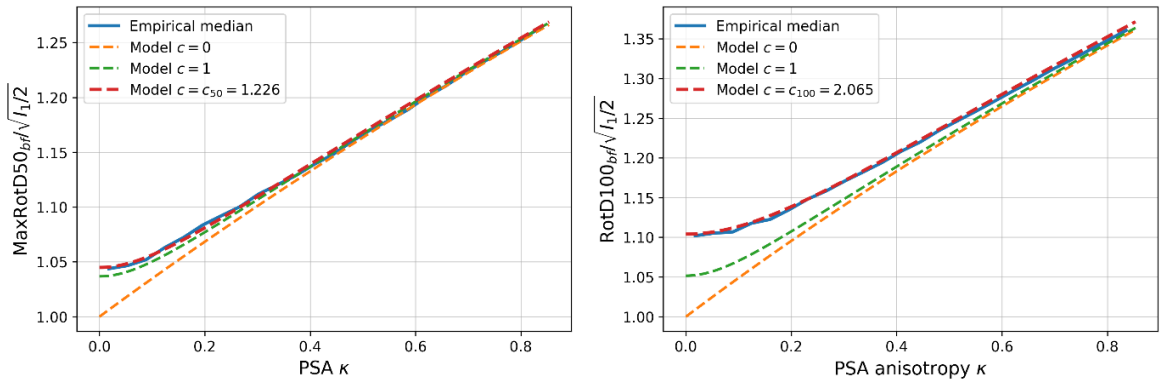

Figure 5. Median empirical amplification compared with closed-form predictions for reference values $c = 0$, $c = 1$, and the calibrated constants for MaxRotD50 (left) and RotD100 (right).

5.3 Evaluation of the closed-form equations

5.4 Bias with oscillator period

To quantify systematic differences between the closed-form expressions and dense directional sampling, we define logarithmic residual

$$r(T) = \ln\left(\frac{\mathrm{IM}_{bf}(T)}{\mathrm{IM}_{cf}(T)}\right),$$

where $\mathrm{IM}_{bf}(T)$ denotes the rotation-invariant measure obtained from dense directional evaluation and $\mathrm{IM}_{cf}(T)$ denotes the corresponding closed-form prediction. For ease of interpretation, results are reported in terms of percentage bias,

$$b(T) = 100\left(\exp(r(T)) - 1\right) = 100\left(\frac{\mathrm{IM}_{bf}(T)}{\mathrm{IM}_{cf}(T)} - 1\right).$$

Figure 6 shows the percentage bias as a function of oscillator period for RotD50, MaxRotD50, and RotD100. The median bias remains small over the full period range, generally within ±1–2%. No systematic drift with period is observed. This confirms that the assumptions underlying the derivation do not introduce period-dependent bias. The spread of bias differs systematically across operators. RotD50 exhibits the largest dispersion, with a wider 16th–84th percentile band. MaxRotD50 shows intermediate dispersion and RotD100 the smallest. This hierarchy is consistent with the conservative truncation bounds in Figure 4.

For MaxRotD50 and RotD100, three closed-form variants are shown: a deterministic-only model with $c = 0$, a reference model with $c = 1$ corresponding to the nominal stochastic amplitude inferred from Equation A19 in Appendix A, and the calibrated model with operator-specific values $c_{50} = 1.226$ and $c_{100} = 2.065$. Here a 0 value of c corresponds to isotropic peak factor, and c equal 1 corresponds to no inflation in anisotropy due to nonlinear mapping between peak factor fluctuations and PSA.

The $c = 0$ curves exhibit a systematic positive bias. This means constant peak factor assumption underestimates MaxRotD50 and RotD100. Introducing stochastic anisotropy through a nonzero c substantially reduces this bias. Moving from $c = 0$ to $c = 1$ produces a reduction in bias for both max-type measures. This shows that the dominant correction arises from the introduction of a stochastic anisotropy amplitude ρ_0. The calibrated values c_{50} and c_{100} further refine this reduction in bias. Geometry alone cannot reproduce this behaviour.

Figure 6 shows the residual trends with period. The calibrated model provides the most consistent bias reduction for RotD100. For MaxRotD50, the difference between the $c = 1$ and calibrated curves is smaller.

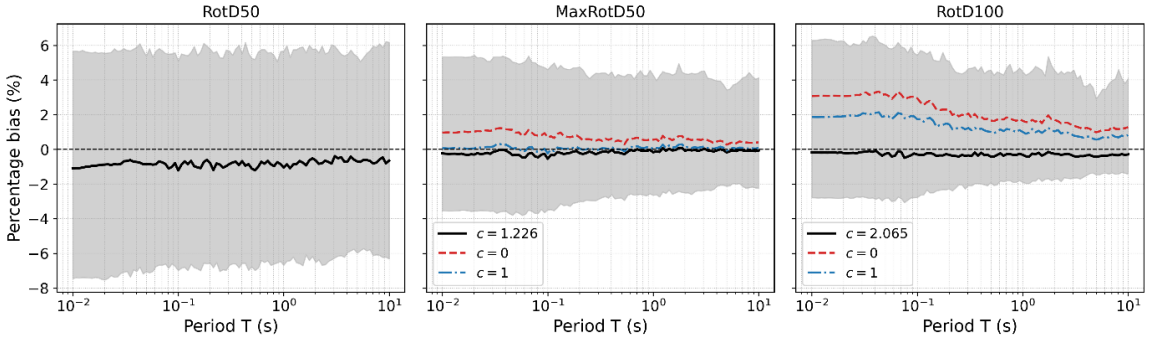

Figure 6 Percentage bias of the closed-form predictions relative to dense directional sampling as a function of oscillator period for RotD50, MaxRotD50, and RotD100. Solid black curves show the median bias across records, and shaded regions indicate the 16th–84th percentile range.

We next examine the prediction bias conditioned on the anisotropy parameter κ. Conditioning on κ isolates the effect of stochastic peak factor variability and identifies the regimes in which quadrature corrections are most influential. Figure 7 shows the percentage bias of closed-form solutions relative to densely sampled angular estimates. The dominant source of bias in the closed-form predictions is in the low-anisotropy regime. Neglecting quadrature anisotropy ($c = 0$) leads to a clear positive bias at small κ. Introducing a nominal quadrature contribution ($c = 1$) reduces this bias but does not fully eliminate it, particularly for RotD100. The calibrated models effectively remove the low-κ bias while preserving consistency across the full range of anisotropy. At larger κ, where deterministic anisotropy dominates, all model variants converge and the bias becomes negligible. These results indicate that κ is a physically meaningful and practically useful descriptor of ground-motion directionality. The success of a simple, κ-dependent effective anisotropy formulation underscores that much of the complexity of directional ground-motion variability can be reduced to a small number of interpretable parameters.

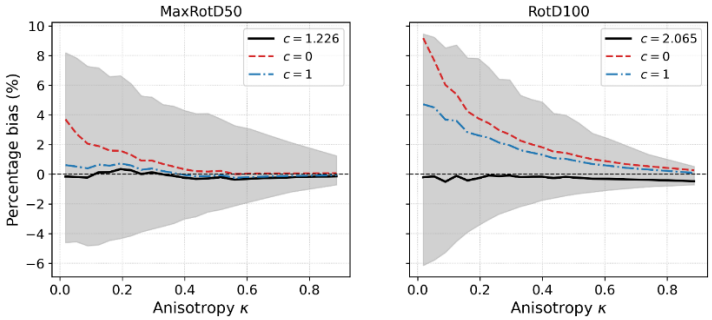

Figure 7. Percentage bias of the closed-form predictions for MaxRotD50 (left) and RotD100 (right) relative to dense directional sampling, conditioned on the anisotropy parameter κ. Solid black curves show the median bias across all records, shaded regions indicate the 16th–84th percentile range, and dashed curves correspond to alternative model variants ($c = 0$ and $c = 1$). The calibrated models ($c = 1.226$ for MaxRotD50 and $c = 2.065$ for RotD100) effectively remove the systematic low-κ bias while preserving consistency across the full anisotropy range.

5.5 Record level performance of the closed form measures

Rotation-invariant measures are commonly used in ground-motion models and hazard applications, where maintaining relative amplitudes across records is as important as achieving unbiased central estimates. To assess record-level performance, we examine agreement between closed-form predictions and dense directional sampling at representative periods. Figure 8 shows scatter plots of dense angular sampling and closed-form estimates at three representative periods ($T = 0.1$, 1.0, and 5.0 s). The scatter clouds tightly follow the 1:1 line over several orders of magnitude in response amplitude.

We next examine a small set of worst-case records. Figure 9 compares closed-form rotation-invariant spectra with dense directionally sampled estimates for the three records exhibiting the largest maximum absolute log-residuals across period. Even for these worst-case examples, deviations are small confined to narrow period bands, mostly at very short periods. This result provides strong evidence that the proposed closed-form expressions preserve not only median trends and overall variability, but also the record-specific spectral characteristics of individual ground motions.

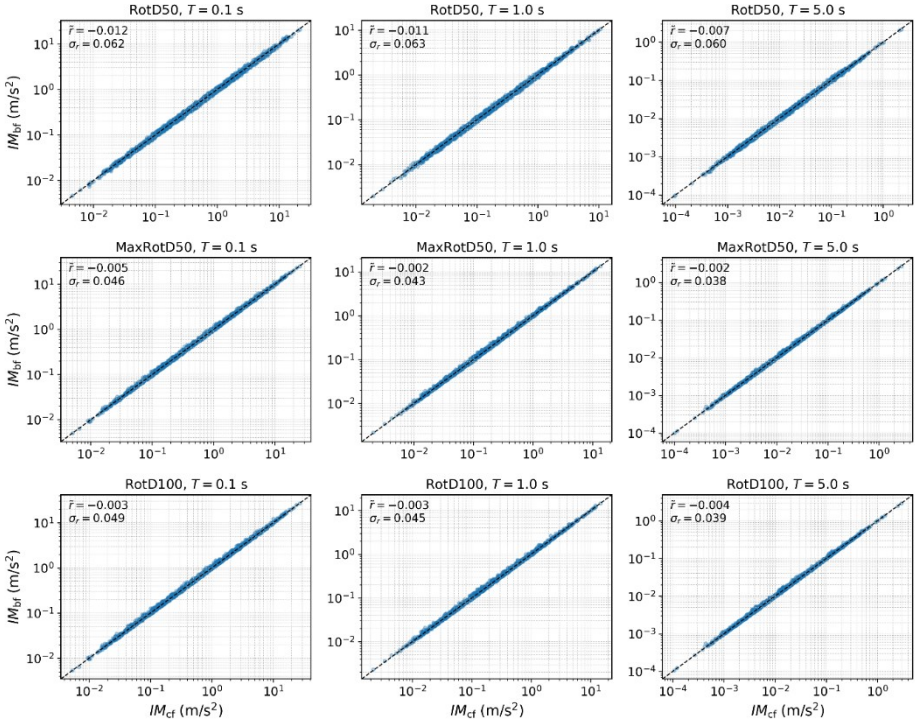

Figure 8 Record-level comparison between dense directional sampling and closed-form predictions for RotD50 (top row), MaxRotD50 (middle row), and RotD100 (bottom row) at representative periods $T = 0.1$, 1.0, and 5.0 s. Each panel shows IM_{bf} versus IM_{cf} on logarithmic axes, with the 1:1 line indicated. Annotations report the median and standard deviation of the log-residual $r = \ln(IM_{bf}/IM_{cf})$. The tight alignment along the 1:1 line across all measures and periods demonstrates that the closed-form expressions preserve record-to-record variability with only small residual scatter.

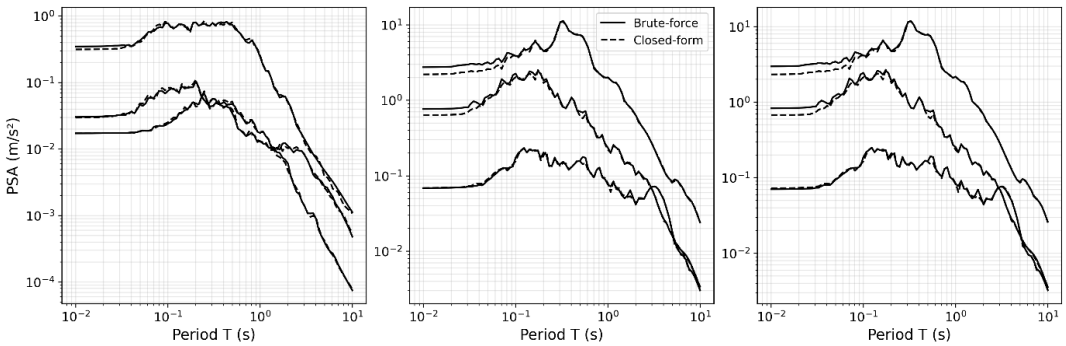

Figure 9. Worst-case record-level comparison of angularly sampled (solid lines) and closed-form (dashed lines) rotation-invariant response spectra for RotD50, MaxRotD50, and RotD100. For each operator, the three records with the largest maximum absolute log-residual across period are shown.

5.6 Residuals as a function of source and source-site parameters

We present the dependence of closed-form prediction errors as a function of moment magnitude (Mw) and Joyner–Boore distance (Rjb) in Figure 10. It shows record-level log-residuals, denoted as η, evaluated at $T \approx 0.1$, 1.0, and 5.0 s. Individual records are plotted as grey points, while black curves indicate binned median residuals to highlight any systematic trends. The median residuals remain close to zero with no discernible dependence on either magnitude or distance.

5.7 Hidden structure in rotation-invariant ratios: the role of κ

Previous studies have reported smooth, period-dependent relationships for ratios of rotation-invariant response spectra, such as MaxRotD50/RotD50 and RotD100/RotD50, obtained by averaging over large numbers of ground-motion records (e.g., Boore & Kishida, 2017; Poulos & Miranda, 2022). While these relationships are widely used, their apparent period dependence has not been linked to an underlying physical control variable.

Figure 11 examines these ratios at the record level by conditioning explicitly on the directional anisotropy parameter κ. When stratified by κ, the ratios exhibit clear and systematic separation, with higher-κ records producing consistently larger ratios across all periods. In contrast, records with low κ show nearly period-independent behaviour. The pooled median curves closely match the κ-marginalized empirical models from the literature, confirming consistency with prior studies.

Ratios of rotation-invariant response spectra, such as RotD100/RotD50, have often been used as empirical indicators of ground-motion directionality. This practice is intuitive, as such ratios increase when motion is strongly polarized and decrease when motion is nearly isotropic. The results presented here clarify the basis for this behaviour and motivate a more direct interpretation of directional effects in terms of the anisotropy parameter κ. Our results show that ratios such as RotD100/RotD50 are governed primarily by κ. They act as derived summaries of the underlying directional structure of the motion. The apparent period dependence of these ratios arises from aggregation over records with different κ values. $\kappa$is the hidden controlling variable.

The left panel of Figure 12 shows RotD100/RotD50 as a function of κ for all record–period samples, with cases satisfying $\kappa < 0.1$ and RotD100/RotD50 > 1.2 highlighted. While the ratio increases on average with κ, a substantial number of samples with low κ show elevated ratios. The right panel compares the distributions of RotD100/RotD50 for low-κ and higher-κ regimes, demonstrating significant overlap between the two populations and confirming that large ratios are not unique to strongly anisotropic motions.

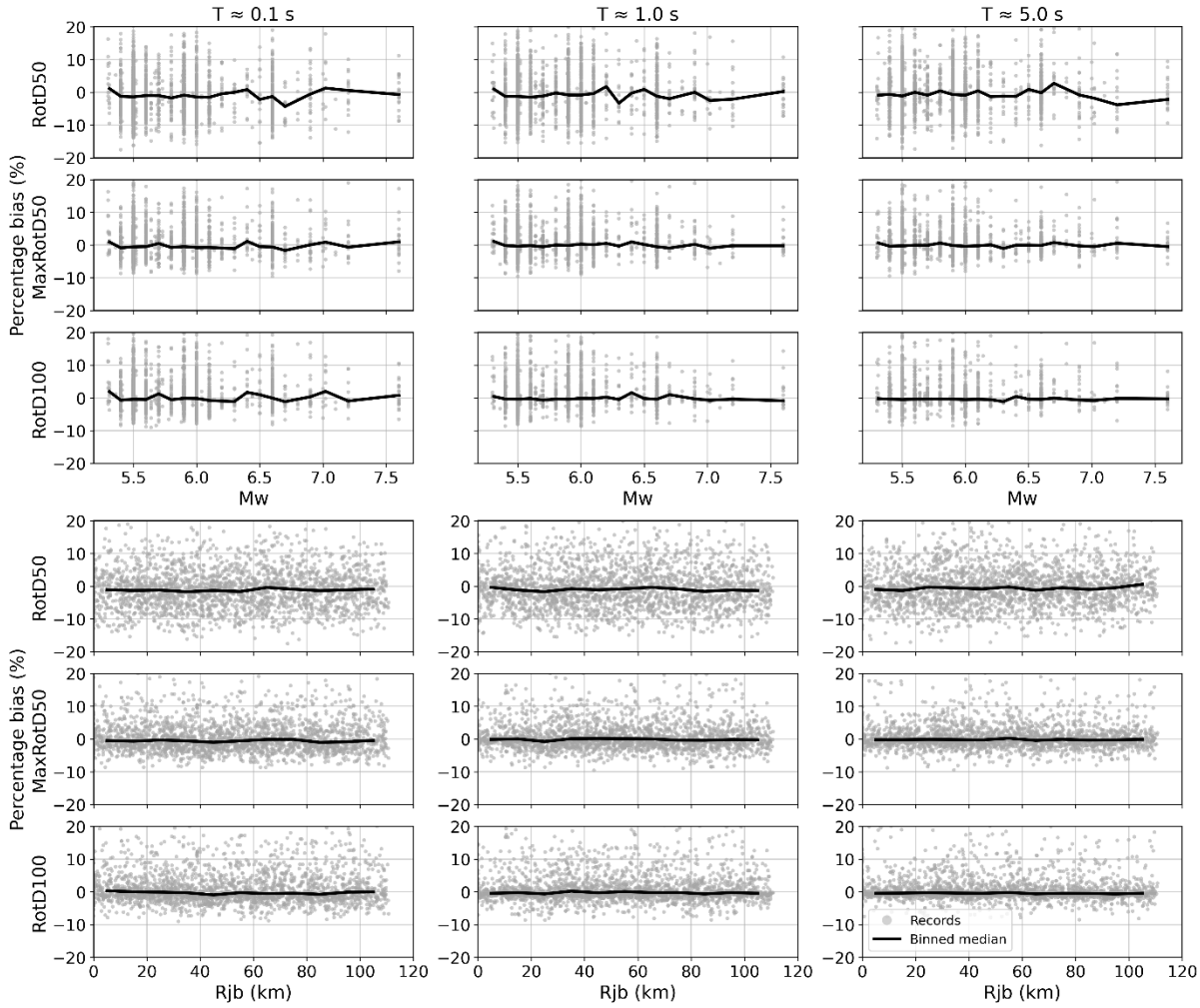

Figure 10. Residual bias of closed-form rotation-invariant response spectra as a function of moment magnitude (Mw) and Joyner–Boore distance (Rjb) for RotD50, MaxRotD50, and RotD100. Log-residuals are evaluated at representative periods T ≈ 0.1, 1.0, and 5.0 s. The top three rows show residuals versus Mw, and the bottom three rows show residuals versus Rjb. Grey points indicate individual records, and black curves denote binned median residuals.

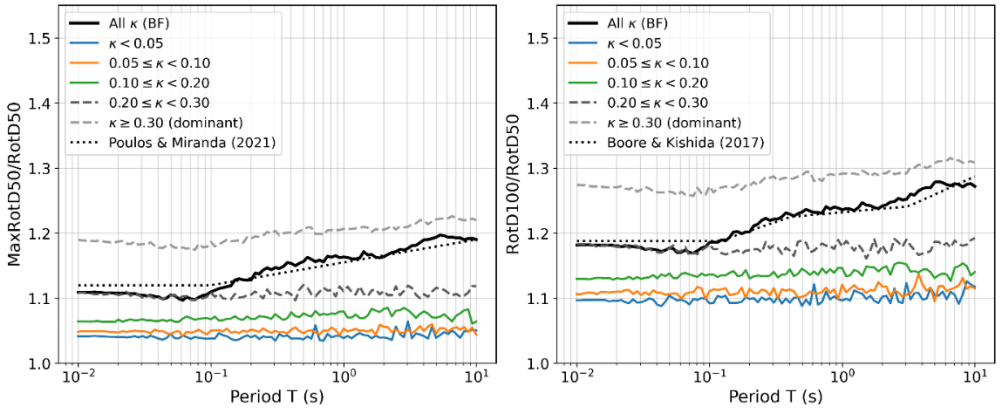

Figure 11. κ-stratified ratios MaxRotD50/RotD50 (left) and RotD100/RotD50 (right) as functions of period. Coloured curves show κ-conditioned medians, while the thick black curve denotes the pooled median. Empirical models from Poulos and Miranda (2021) and Boore and Kishida (2017) are shown for reference.

These observations provide a clear explanation for why amplification ratios have often been found to approach their upper bound even in motions that appear weakly polarized. RotD100 is controlled by extreme directional peaks and is therefore sensitive to localized, moderately polarized pulses that may occupy only a small portion of the record. Such pulses are sufficient to inflate the maximum relative to the median. This behaviour is intrinsic to

peak-based ratios and reflects stochastic peak-factor variability rather than persistent directional anisotropy. By contrast, κ is derived from the squared PSA in the RMS principal basis and quantifies the amplitude of directional variation in the response spectrum itself. As such, κ characterizes persistent directional structure rather than isolated extremes.

Directional effects in ground motions are known to arise from identifiable physical mechanisms, including rupture directivity, wave propagation effects, and site-specific response. The choice of directionality metric is critical to investigate such causal factors or to classify ground motions according to their degree of physical anisotropy. If RotD100/RotD50 is used as directionality metric, ground motions that are physically dissimilar may be grouped together, obscuring the relationship between observed directionality and its underlying source or site-related causes.

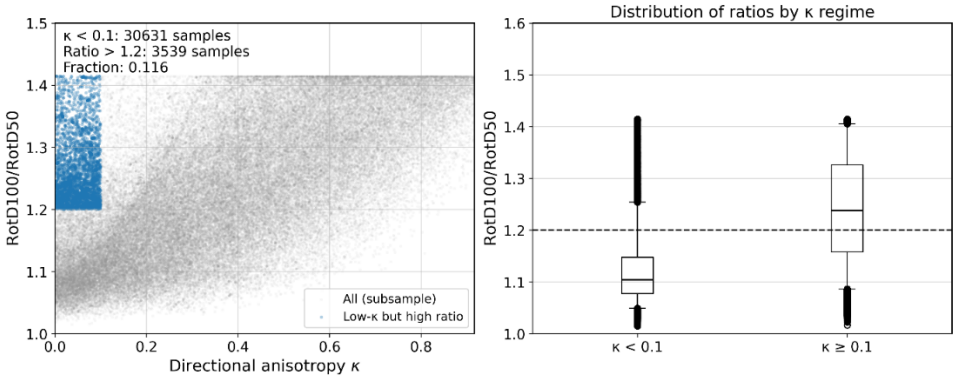

Figure 12. Evidence of false positives when using RotD100/RotD50 as a directionality measure. Left panel shows RotD100/RotD50 versus the directional anisotropy parameter κ for all record–period samples; blue points highlight cases with κ < 0.1 and RotD100/RotD50 > 1.2. Right panel compares the distributions of RotD100/RotD50 for low-κ and higher-κ regimes. A substantial fraction of nearly isotropic motions (low κ) exhibit elevated ratios due to stochastic peak selection, demonstrating that large amplification ratios do not uniquely indicate strong directional anisotropy and motivating κ as a more robust descriptor of directionality.

Overall, apparent directional amplification may not reliably indicate the presence or strength of directional mechanisms, hindering efforts to attribute observed behaviour to specific physical processes. By contrast, κ provides a cleaner basis for record-level classification and for investigating causal links between ground-motion directionality and its physical origins. Interpreting rotation-invariant ratios through κ helps disentangle physical anisotropy from stochastic variability and preserves the causal structure necessary for meaningful interpretation. This distinction is essential for physical interpretation.

6 Discusssion

The results of this study clarify an important but often overlooked distinction between rotation invariance and scalar representation. Rotation-invariant measures are invariant to the choice of coordinate system, but they are not necessarily direction-free summaries of two-dimensional ground motion. As shown here, rotation-invariant measures act as directional selection operators on a structured angular response field, and different operators preserve different aspects of directional variability.

Median-type measures such as RotD50 suppress directional extremes and behave similarly to conventional scalar averages. Max-type measures, on the other hand, explicitly encode directional selection and therefore retain information about directional modulation. Treating all rotation-invariant measures as interchangeable scalar proxies can therefore obscure the physical meaning of the retained directional information and lead to inconsistent interpretations when such measures are used in bidirectional structural analysis or orthogonal demand combination rules. This perspective helps reconcile long-standing observations that different rotation-invariant measures exhibit different levels of conservatism and dispersion, even when derived from the same ground-motion records.

By treating directional PSA as a low-dimensional stochastic field, this study shows that commonly used rotation-invariant measures are governed by a small number of directional invariants rather than by dense angular sampling. Dense angular sampling is therefore not required to approximate RotD50, MaxRotD50, or RotD100, provided that the dominant angular structure of the response is captured. It is noted that RotD100 can be calculated directly from the vector norm of the response time history (Rupakhety and Sigbjörnsson, 2013) to as recorded

ground motion. The motivation for its closed-form approximation here is computational efficiency, but clarification. It exposes the structure of RotD100 and its relationship to other RotDnn measures.

Max-type rotation-invariant measures cannot be represented solely through geometric information derived from an orthogonal component pair. Even when deterministic directional modulation is weak, stochastic variability in directional peak factors produces effective anisotropy that influences extreme-direction selection. The effective anisotropy closure introduced here provides a compact empirical way to account for this unresolved variability while preserving interpretability and avoiding overfitting.

This study identifies the PSA anisotropy parameter κ as a latent variable that organizes the behaviour of rotation-invariant measures. When conditioned on κ, rotation-invariant ratios collapse onto simple, nearly period-independent relationships, and the apparent period dependence observed in pooled empirical models largely disappears. This indicates that κ, rather than oscillator period alone, is the primary control on directional selection effects.

In current ground motion modelling practice, variability associated with directionality is typically absorbed into the aleatory variability term, implicitly treating it as unstructured noise. The results of this study suggest that such an approach may obscure a physically meaningful component of variability. The parameter κ captures a systematic aspect of directional structure that governs how two-dimensional ground motion is mapped into rotation-invariant scalar measures through operator-specific selection. Treating this structure as purely aleatory neglects the fact that different records, even at similar magnitude and distance, occupy distinct directional states with different implications for max-type measures.

From this perspective, κ is more naturally interpreted as a conditioning variable. While the present study does not develop predictive models for κ, the results indicate that κ-aware representations of rotation-invariant measures, or explicit marginalization over κ, may provide a more transparent and physically grounded framework for future GMM development. This distinction is particularly relevant for max-type measures, whose behaviour is shown here to depend on effective anisotropy even when deterministic directional modulation is weak.

Finally, this study focuses on pseudo-spectral acceleration and on the directional structure observed in the ESM dataset. While the empirical findings suggest broad robustness, further investigation is warranted to assess the extent to which the stochastic anisotropy parameters identified here generalize across datasets and tectonic regimes. Establishing such robustness is a necessary step toward incorporating directional structure explicitly into future ground-motion models.

7 Conclusions

This study developed a closed-form framework for commonly used rotation-invariant ground-motion intensity measures by exploiting the low-dimensional directional structure of pseudo-spectral acceleration. Rather than treating rotation invariance as a numerical procedure, the approach interprets rotation-invariant measures as directional selection operators acting on a structured angular response field.

A central contribution is the conceptual clarification that rotation-invariant measures are not statistics of redundant angular samples. The directional PSA field is not a collection of interchangeable observations over orientation, but a structured stochastic field with a small number of controlling degrees of freedom. Rotation-invariant operators transform this directional structure by selecting specific features of the field, rather than averaging away directional information. Differences among RotD50, MaxRotD50, and RotD100 therefore arise from fundamentally different selection objectives. They should not be interpreted interchangeably.

Using a large dataset of ground-motion records from the European Strong-Motion database, the study showed that the directional PSA field is strongly dominated by its first admissible harmonic in squared-PSA space across periods and records. This structure allows rotation-invariant measures to be expressed in terms of a baseline level and an anisotropy amplitude, computable from a single principal orthogonal pair. Median-type measures are primarily controlled by the baseline level, whereas max-type measures are additionally sensitive to directional modulation.

An important finding is that RMS-based geometric information alone is insufficient to characterize max-type rotation-invariant measures when κ is small. In such case, directional variability of peak factors produces amplification that cannot be inferred from RMS geometry alone. The resulting closed-form expressions reproduce rotation-invariant spectra obtained from dense angular sampling with small bias and modest dispersion across periods and anisotropy levels, while avoiding the computational cost and opacity of numerical rotation.

Beyond providing practical closed-form approximations, the results establish κ as a meaningful latent variable governing directional modulation and directional selection in rotation-invariant measures. This perspective provides a structural basis for interpreting rotation-invariant ratios, explains why such ratios can be elevated even in weakly anisotropic records, and offers a foundation for future κ-aware probabilistic modelling and interpretation of scalar intensity measures in hazard and design applications. Recognizing this structure clarifies what rotation-invariant measures retain, what they suppress, and how they should be interpreted in practice.

Appendix A. Derivation of closed-form RotD equations

A.1 Directional response and RMS principal axes

Let us consider a SDOF oscillator with period T and circular frequency ω and damping ratio 5%. Let $d_1(t)$ and $d_2(t)$ represent the relative displacement response of the oscillator to as-recorded horizontal components of ground motion record. The pseudo-acceleration response is $a_i(t) = \omega^2 d_i(t), \quad i = 1,2$. The acceleration response vector is written as $\mathbf{a}(t) = \left(a_1(t), a_2(t)\right)^{\mathrm{T}}$ With θ denoting the orientation of the horizontal response axis, the directional response is

$$\mathbf{u}(\theta) = \begin{pmatrix} \cos\theta \\ \sin\theta \end{pmatrix}, \qquad a(t,\theta) = \mathbf{u}(\theta)^{\mathrm{T}} \mathbf{a}(t) \tag{A1}$$

Using a time average over the record, we define the response covariance and directional second moment (RMS squared)

$$\mathbf{C} = \mathbb{E}\left[\mathbf{a}(t)\,\mathbf{a}(t)^{\top}\right], \qquad \sigma_a^2(\theta) = \mathbb{E}\left[a(t,\theta)^2\right] = \mathbf{u}(\theta)^{\top}\,\mathbf{C}\,\mathbf{u}(\theta) \tag{A2}$$

Let $\lambda_1 \geq \lambda_2 \geq 0$ be eigenvalues of $\mathbf{C}$ and θ_0 the eigenvector direction of λ_1. Then the RMS field is exactly elliptical:

$$\sigma_a^2(\theta) = \bar{\sigma}_a^2\left(1 + \Delta\cos 2(\theta - \theta_0)\right), \qquad \bar{\sigma}_a^2 = \frac{1}{2}(\lambda_1 + \lambda_2), \qquad \Delta = \frac{\lambda_1 - \lambda_2}{\lambda_1 + \lambda_2} \tag{A3}$$

Here θ_0 identifies the dominant rms axis and Δ quantities rms anisotropy. The $\cos 2\theta$ form is forced by π-periodicity. This interpretation is a measure of rectilinearity of the RMS response. The quadratic form of the covariance matrix is positive semidefinite with shape and orientation represented by an ellipsoid which best fits the data points in the least-squares sense (Flinn, 1965).

A.2 Directional PSA and peak factor

Directional PSA is defined as

$$\mathrm{PSA}(\theta) = \max_t \left|a(t,\theta)\right| \tag{A4}$$

We introduce the peak factor $p(\theta) := PSA(\theta) / \sigma_a(\theta)$, and model it in log space as:

$$\ln p(\theta) = \mu_p + \varepsilon(\theta), \qquad \varepsilon(\theta + \pi) = \varepsilon(\theta), \qquad \operatorname*{med}_{\theta \in [0,\pi)} \varepsilon(\theta) = 0 \tag{A5}$$

Here $\varepsilon(\theta)$ captures direction peak-factor variation after removing rms variation. Empirical evidence (Paper 1) shows that it is (i) dominated by the first admissible harmonic, (ii) approximately isotropic (iii) the first harmonic coefficients are near-Gaussian and independent (iv) the phase of the harmonic is broadly uniform.

Three rotation invariant PSA measures of interest are addressed

$$\mathrm{RotD50} = \underset{\theta\in[0,\pi)}{\mathrm{med}}\, PSA(\theta) \tag{6a}$$

$$\mathrm{MaxRotD50} = \underset{\theta\in[0,\pi)}{\mathrm{med}} \max\left\{PSA(\theta), PSA(\theta+\frac{\pi}{2})\right\} \tag{6b}$$

$$\mathrm{RotD100} = \max_{\theta\in[0,\pi)} PSA(\theta) \tag{6c}$$

A3 Squared-space operators

We define the squared PSA field as $S(\theta) := PSA^2(\theta)$. Using $PSA(\theta) = \sigma_a(\theta)\, p(\theta)$ and the peak factor model from (A5) we get

$$S(\theta) = \sigma_a^2(\theta)\exp\left\{2\mu_p + 2\varepsilon(\theta)\right\} \tag{A7}$$

We define squared-space rotation-invariant operators as

$$F_{50}(S) = \underset{\theta\in[0,\pi)}{\mathrm{med}}\, S(\theta) \tag{A8a}$$

$$F_{100}(S) = \max_{\theta\in[0,\pi)} S(\theta) \tag{A8b}$$

$$F_M(S) = \underset{\theta\in[0,\pi)}{\mathrm{med}} \max\left\{S(\theta), S(\theta+\frac{\pi}{2})\right\} \tag{A8c}$$

Since $\sqrt{\cdot}$ is strictly increasing,

$$\mathrm{RotD50} = \sqrt{F_{50}(S)}, \qquad \mathrm{RotD100} = \sqrt{F_{100}(S)}, \qquad \mathrm{MaxRotD50} = \sqrt{F_M(S)} \tag{A9}$$

A.4 PSA invariants from the rms principal orthogonal pair

We define $S_a := S(\theta_0)$ and $S_b := S(\theta_0 + \pi/2)$. Then using the ordered pair $(S_1, S_2) = \left(\max\{S_a, S_b\}, \min\{S_a, S_b\}\right)$, we define two invariants as

$$I_1 := S_1 + S_2, \qquad \kappa := \frac{S_1 - S_2}{S_1 + S_2}, \quad 0 \le \kappa < 1 \tag{A10}$$

Here κ serves as a dimensionless measure of anisotropy of PSA in the principal directions.

A.5 Fourier structure of $S(\theta)$

Because $S(\theta)$ is π-periodic, it admits the Fourier expansion

$$S(\theta) = a_0 + \sum_{n\ge 1}\left(a_n \cos 2n\theta + b_n \sin 2n\theta\right)$$

Empirical evidence (Paper 1) shows that the peak-factor fluctuation field is dominated by its first admissible harmonic. This implies that the induced directional variation in $S(\theta)$ is well-approximated by its first-harmonic projection, with higher harmonics treated as a bounded remainder. We therefore define the first-harmonic projection and remainder as

$$S(\theta) = S_0(\theta) + r_s(\theta), \qquad S_0(\theta) := a_0 + a_1 \cos 2\theta + b_1 \sin 2\theta \tag{A11}$$

and summarize the neglected content by a single amplitude

$$\delta_s = \| r_s \|_\infty = \sup_{\theta \in [0,\pi)} \left(S(\theta) - S_0(\theta) \right) \tag{A12}$$

Here δ_s is the maximum contribution of higher harmonics and any mismatch due to nonlinear map $\exp\{2\varepsilon(\theta)\}$. If δ_s is small relative to the overall level a_0, the first-harmonic approximation is accurate for the rotation operators.

A.6 Exact rotation-invariant operators under single-harmonic field

The first-harmonic field can be written in amplitude-phase form as

$$S_0(\theta) = a_0 + R\cos(2\theta - \varphi), \qquad R = \sqrt{a_1^2 + b_1^2}$$

The phase φ does not affect rotation-invariant operators because the domain $\theta \in [0, \pi)$ is shift invariant. Using the identities for $\Phi \sim \mathrm{Unif}[0, \pi)$

$$\operatorname*{med}_{\Phi \in [0,\pi)} \left(\cos\Phi \right) = 0, \qquad \operatorname*{med}_{\Phi \in [0,\pi)} \left(|\cos\Phi| \right) = \frac{1}{\sqrt{2}}, \qquad \max_{\Phi \in [0,\pi)} \cos\Phi = 1$$

we obtain exact squared-space operators

$$F_{50}(S_0) = a_0, \qquad F_M(S_0) = a_0 + \frac{R}{\sqrt{2}}, \qquad F_{100}(S_0) = a_0 + R$$

Then using (A8) the first-harmonic approximations can be written as

$$\mathrm{RotD50}_0 = \sqrt{a_0}, \qquad \mathrm{MaxRotD50}_0 = \sqrt{a_0 + \frac{R}{\sqrt{2}}}, \qquad \mathrm{RotD100}_0 = \sqrt{a_0 + R} \tag{A13}$$

A.7 Relating first-harmonic parameters to the PSA-space invariants

In the RMS principal basis, the orthogonal directions correspond to $\theta = 0$ and $\theta = \pi/2$: so from (A7) we have

$$S_0(0) = a_0 + a_1, \qquad S_0\left(\frac{\pi}{2}\right) = a_0 - a_1$$

Matching these to the ordered orthogonal pair (S_1, S_2) yields

$$a_0 = \frac{S_1 + S_2}{2} = \frac{I_1}{2}, \qquad a_1 = \frac{S_1 - S_2}{2} = \frac{I_1}{2}\kappa \tag{A14}$$

The coefficient b_1 cannot be identified from a single orthogonal pair, it is a quadrature (out-of-phase) component. To address this, we define the normalized coefficients

$$\kappa_\perp = \frac{b_1}{a_0}, \qquad \kappa_{\mathrm{tot}} = \frac{R}{a_0} = \sqrt{\kappa^2 + \kappa_\perp^2} \tag{A15}$$

Substituting (A14) and (A15) in (A11) yields

$$\mathrm{RotD50}_0 = \sqrt{\frac{I_1}{2}}, \qquad \mathrm{MaxRotD50}_0 = \sqrt{\frac{I_1}{2}\left(1+\frac{\kappa_{\mathrm{tot}}}{\sqrt{2}}\right)}, \qquad \mathrm{RotD100}_0 = \sqrt{\frac{I_1}{2}\left(1+\kappa_{\mathrm{tot}}\right)}$$

At this stage, κ_{tot} is unknown due to unobserved quadrature component $\kappa_{\perp}$. In the following we explore its estimation based on empirical evidence.

A.8 Empirical closure of unobserved quadrature component

Empirical evidence (Paper 1) suggests that the orientation (phase) of the first-harmonic anisotropy is broadly spread and consistent with a uniform random angle, and that amplitude and phase are approximately independent. If $\varepsilon(\theta)$ is first-harmonic dominated with amplitude ρ, the impact of peak-factor fluctuations in the unobserved quadrature of first-harmonic representation of $S(\theta)$ is proportional to ρ. The exact mapping of this effect is not known because of exponential transformation, see (A7). It is assumed here that such nonlinear mapping and effect of higher harmonics can be modelled by a simple inflation factor $c \geq 1$. If we define a normalized coefficient vector as

$$\mathbf{k} = \left(\frac{a_1}{a_0}, \frac{b_1}{a_0}\right) = \left(\kappa, \kappa_{\perp}\right) \tag{A16}$$

and decompose into two components, one coming from the rms ellipse geometry and the other from the peak-factor fluctuations including the inflation factor, we have the following representation

$$\mathbf{k} = (\kappa, 0) + c\rho(\cos\Phi, \sin\Phi), \qquad \Phi \sim \mathrm{Unif}[0, \pi), \qquad \Phi \perp \rho \tag{A17}$$

With this representation, the norm of anisotropy vector can be written as

$$\kappa_{\mathrm{tot}} = \| \mathbf{k} \| = \sqrt{\kappa^2 + (c\rho)^2 + 2\kappa(c\rho)\cos\Phi} \tag{A18}$$

For a given ground motion record (fixed κ and ρ), the median κ_{tot} can be evaluated as

$$\underset{\Phi\in[0,\pi)}{\mathrm{med}}\left(\kappa_{\mathrm{tot}} | \kappa, \rho\right) = \sqrt{\kappa^2 + (c\rho)^2} \tag{A19}$$

This requires, for every record, an additional parameter to quantify the quadrature anisotropy. Given the empirical observations from (Rupakhety and Hernández-Aguirre, 2026), we propose an effective anisotropy. It is interpreted by a dataset level floor, and is defined as

$$\kappa_{\mathrm{eff}} := \sqrt{\kappa^2 + (c\rho_0)^2}, \quad \rho_0 := \mathrm{med}(\rho) \tag{A20}$$

Under Rayleigh distribution of ρ with scale S (Rupakhety and Hernández-Aguirre, 2026)

$$\rho_0 = s\sqrt{2\ln 2}$$

Defining $\mathrm{MAD}(\rho) = \mathrm{med}\left(|\rho - \rho_0|\right)$, since $x \mapsto \sqrt{x^2 + (cx)^2}$ is c-Lipschitz in x,

$$\mathrm{med}\left(\sqrt{\kappa^2 + (c\rho)^2}\right) - \sqrt{\kappa^2 + (c\rho_0)^2} \leq c\,\mathrm{MAD}(\rho)$$

quantifies the approximation introduced by using a dataset level representation of ρ.

A.9 Final closed forms with residual

Using κ_{eff} as a median-equivalent surrogate for total anisotropy, the rotation invariant measures can be written as

$$\mathrm{RotD50} = \sqrt{\frac{I_1}{2}} + R_{50} \tag{A21a}$$

$$\mathrm{MaxRotD50} = \sqrt{\frac{I_1}{2}\left(1 + \frac{\kappa_{\mathrm{eff}}}{\sqrt{2}}\right)} + R_M \tag{A21b}$$

$$\mathrm{RotD100} = \sqrt{\frac{I_1}{2}\left(1 + \kappa_{\mathrm{eff}}\right)} + R_{100} \tag{A21c}$$

where the residuals R are controlled by two measurable effects.

$$\mathcal{R} \approx \mathcal{R}^{(\mathrm{harm})} + \mathcal{R}^{(\mathrm{floor})}$$

The effect of neglected higher harmonics in $S(\theta)$ is controlled by $\delta_s = \| S - S_0 \|_\infty$. For $F \in \{F_{50}, F_{100}, F_M\}$

$$F(S) - F(S_0) \le \delta_s$$

Mapping from squared PSA to PSA space used the identity

$$\left|\sqrt{x} - \sqrt{y}\right| = \frac{|x - y|}{\sqrt{x} + \sqrt{y}}$$

If $F(S)$ and $F(S_0)$ are bounded below by $m > 0$, the

$$\sqrt{F(S)} - \sqrt{F(S_0)} \le \frac{\delta_s}{2\sqrt{m}}$$

Floor representation of ρ at the dataset level introduces a median error bounded by $c\mathrm{MAD}(\rho)$

References

American Society of Civil Engineers. (2022). *Minimum Design Loads and Associated Criteria for Buildings and Other Structures (ASCE/SEI 7-22)*. https://doi.org/10.1061/9780784414248

Ancheta, T. D., Darragh, R. B., Stewart, J. P., Seyhan, E., Silva, W. J., Chiou, B. S.-J., Wooddell, K. E., Graves, R. W., Kottke, A. R., Boore, D. M., Kishida, T., & Donahue, J. L. (2014). NGA-West2 Database. *Earthquake Spectra*, *30*(3), 989–1005. https://doi.org/10.1193/070913EQS197M

Beyer, K., & Bommer, J. J. (2006). Relationships between Median Values and between Aleatory Variabilities for Different Definitions of the Horizontal Component of Motion. *Bulletin of the Seismological Society of America*, *96*(4 A), 1512–1522. https://doi.org/10.1785/0120050210

Boore, D. M. (2010). Orientation-Independent, Nongeometric-Mean Measures of Seismic Intensity from Two Horizontal Components of Motion. *Bulletin of the Seismological Society of America*, *100*(4), 1830–1835. https://doi.org/10.1785/0120090400

Boore, D. M., & Kishida, T. (2017). Relations between Some Horizontal-Component Ground-Motion Intensity Measures Used in Practice. *Bulletin of the Seismological Society of America*, *107*(1), 334–343. https://doi.org/10.1785/0120160250

Boore, D. M., Watson-Lamprey, J., & Abrahamson, N. A. (2006). Orientation-Independent Measures of Ground Motion. *Bulletin of the Seismological Society of America*, *96*(4A), 1502–1511. https://doi.org/10.1785/0120050209

Bozorgnia, Y., Abrahamson, N. A., Atik, L. A., Ancheta, T. D., Atkinson, G. M., Baker, J. W., Baltay, A., Boore, D. M., Campbell, K. W., Chiou, B. S.-J., Darragh, R., Day, S., Donahue, J., Graves, R. W., Gregor, N., Hanks, T., Idriss, I. M., Kamai, R., Kishida, T., … Youngs, R. (2014). NGA-West2 Research Project. *Earthquake Spectra*, *30*(3), 973–987. https://doi.org/10.1193/072113EQS209M

CEN. (2004). *Eurocode 8: Design of structures for earthquake resistance – Part 1: General rules, seismic actions and rules for buildings. EN 1998-1:2004*. European Committee for Standardization.

Chiou, B.-J., & Youngs, R. R. (2008). An NGA Model for the Average Horizontal Component of Peak Ground Motion and Response Spectra. *Earthquake Spectra*, *24*(1), 173–215. https://doi.org/10.1193/1.2894832

Flinn, E. A. (1965). Signal analysis using rectilinearity and direction of particle motion. *Proceedings of the IEEE*, *53*(12), 1874–1876. https://doi.org/10.1109/PROC.1965.4462

Lanzano, G., Sgobba, S., Luzi, L., Puglia, R., Pacor, F., Felicetta, C., D'Amico, M., Cotton, F., & Bindi, D. (2019). The Pan-European Engineering Strong Motion (ESM) Flatfile: Compilation Criteria and Data Statistics. *Bulletin of Earthquake Engineering*, *17*(2), 561–582. https://doi.org/10.1007/s10518-018-0480-z

Luzi, L., Puglia, R., Russo, E., D'Amico, M., Felicetta, C., Pacor, F., Lanzano, G., Çeken, U., Clinton, J., Costa, G., Duni, L., Farzanegan, E., Gueguen, P., Ionescu, C., Kalogeras, I., Özener, H., Pesaresi, D., Sleeman, R., Strollo, A., & Zare, M. (2016). The Engineering Strong-Motion Database: A Platform to Access Pan-European Accelerometric Data. *Seismological Research Letters*, *87*(4), 987–997. https://doi.org/10.1785/0220150278

Poulos, A., & Miranda, E. (2022). Proposal of orientation-independent measure of intensity for earthquake-resistant design. *Earthquake Spectra*, *38*(1), 235–253. https://doi.org/10.1177/87552930211038240

Ramadan, F., Smerzini, C., Lanzano, G., & Pacor, F. (2021). An Empirical Model for the Vertical-to-Horizontal Spectral Ratios for Italy. *Earthquake Engineering and Structural Dynamics*, *50*(15), 4121–4141. https://doi.org/10.1002/eqe.3548

Rupakhety, R., & Sigbjörnsson, R. (2013). Rotation-Invariant Measures of Earthquake Response Spectra. *Bulletin of Earthquake Engineering*, *11*(6), 1885–1893. https://doi.org/10.1007/s10518-013-9472-1

Rupakhety, R., & Sigbjörnsson, R. (2014a). Rotation-Invariant Formulation of Strong Ground-Motion Parameters. *In Proceedings of the Second European Conference on Earthquake Engineering and Seismology*.

Rupakhety, R., & Sigbjörnsson, R. (2014b). Rotation-invariant mean duration of strong ground motion. *Bulletin of Earthquake Engineering*, *12*(2), 573–584. https://doi.org/10.1007/s10518-013-9521-9

Rupakhety, R., Hernández-Aguirre VM (2026) Directional peak factors of strong motion response spectra: a stochastic representation on the circle. Earthquake Spectra (under review)

Shahi, S. K., & Baker, J. W. (2014). NGA-West2 Models for Ground Motion Directionality. *Earthquake Spectra*, *30*(3), 1285–1300. https://doi.org/10.1193/040913EQS097M

Somerville, P. G., Smith, N. F., Graves, R. W., Services, W.-C. F., & Abrahamson, N. A. (1997). Modification of Empirical Strong Ground Motion Attenuation Relations to Include the Amplitude and Duration Effects of Rupture Directivity. *Seismological Research Letters*, *68*(1), 199–222.

Spudich, P., Hellweg, M., & Lee, W. H. K. (1996). Directional topographic site response at Tarzana observed in aftershocks of the 1994 Northridge, California, earthquake: Implications for mainshock motions. *Bulletin of the Seismological Society of America*, *86*(1B), S193–S208. https://doi.org/10.1785/BSSA08601BS193

Stewart, J. P., Abrahamson, N. A., Atkinson, G. M., Baker, J. W., Boore, D. M., Bozorgnia, Y., Campbell, K. W., Comartin, C. D., Idriss, I. M., Lew, M., Mehrain, M., Moehle, J. P., Naeim, F., & Sabol, T. A. (2011). Representation of Bidirectional Ground Motions for Design Spectra in Building Codes. *Earthquake Spectra*, *27*(3), 927–937. https://doi.org/10.1193/1.3608001

Vidale, J. E., Bonamassa, O., & Houston, H. (1991). Directional site resonances observed from the 1 october 1987 whittier narrows, california, earthquake and the 4 october aftershock. *Earthquake Spectra*, *7*(1), 107–125. https://doi.org/10.1193/1.1585616